One-pot Synthesis of Coral-like Ru/Carbon Composites as Superior Electrocatalysts for the Hydrogen Evolution Reaction

Fei Li, Xueguang Wang[*]*, Xiujing Zou, Yuanhua Tao, Shengnan Yue, Xiubin Chen, Xionggang Lu*[*]

State Key Laboratory of Advanced Special Steel, School of Materials Science and Engineering, Shanghai University, Shanghai 200072, China
[*]E-mail: wxg228@shu.edu.cn (X. G. Wang), luxg@shu.edu.cn (X. G. Lu).

A highly active and stable catalyst is crucial for the hydrogen evolution reaction (HER). In this study, a novel coral-like Ru/carbon (Ru/C) electrocatalyst was synthesized via a solvothermal approach with the assistance of 8-hydroxyquinoline (8-HQ). This catalyst exhibited excellent performance for the HER in acidic media. The overpotential of the Ru/C catalyst was 41 mV at a current density of 10 mA/cm^2, the Tafel slope was 46 mV/dec, which was only 12 mV/dec higher than that of the Pt/C catalyst (34 mV/dec). Moreover, the Ru/C catalyst exhibited excellent stability. We believe that this novel Ru/C catalyst is a viable substitute for commercial Pt/C catalysts.

1. INTRODUCTION

With the development of science and technology and the improvement of living standards, the demand for energy is increasing. However, current reserves of fossil energy are limited. Therefore, renewable energy sources must be found to replace the depleting fossil energy sources. Among many renewable energy candidates, hydrogen has attracted considerable attention in recent years because of its high calorific value and zero pollution [1-5]. Currently, hydrogen is industrially produced by methane steam reforming or coal gasification [6]. However, these methods consume very large amounts of energy and emit a large quantity of environmentally harmful and hazardous gases. Therefore, electrochemical water splitting has become the most promising hydrogen production method for its low energy consumption and environmental friendliness [7-10]. The electrolysis of water involves two reactions: the hydrogen evolution reaction (HER) and the oxygen evolution reaction (OER) [11-14]. For the HER process, when the voltage applied to the electrode is greater than the HER overpotential, protons from

the electrolyte are reduced to hydrogen atoms at the cathode and hydrogen gas is thereby generated. Since the HER occurs only when the applied voltage is greater than the reaction overpotential, it is a process that consumes electric energy. Therefore, the development of a suitable catalyst to reduce the overpotential of HER is necessary to realize the industrial utilization of the electrolysis of water for hydrogen production [15-17].

To date, Pt/C has been demonstrated to be the most efficient electrocatalyst for the HER [18-22]. This catalyst reduces the overpotential of the HER to almost zero and has a very small Tafel slope. Unfortunately, the widespread commercialization of Pt/C electrocatalyst is limited by the scarcity and high cost of the precious metal Pt (US\$992 per ounce). Therefore, a new HER catalyst that can replace Pt/C is needed. Current research is mainly focused on two types of catalysts. The first type is nonprecious metal catalysts such as those based on Fe [23,24], Co [25-27], Ni [28-30], or Mo [31-33]. The advantage of these materials is that they are relatively inexpensive and earth-abundant. However, the HER performance of these catalysts is not comparable to that of commercial Pt/C and is far from satisfactory. The second type is precious-metal catalysts such as those based on Pt [34], Pd [35], Ir [36], or Ru [37]. These materials exhibit remarkable catalytic performance, but their practical applications are impeded by their high price and limited availability. Furthermore, most of the current preparation methods for catalysts are complicated, which makes mass production difficult. Thus, great efforts are needed to develop an HER catalyst that is active, stable, and easy to prepare.

In studies of precious-metal catalysts, Ru has been widely recognized for its superior properties. On the one hand, Ru is much less expensive (US\$42 per ounce) but more earth-abundant than Pt. On the other hand, Ru and Pt have similar bond energies as hydrogen (~65 kcal/mol), which enables Ru-based catalysts to reach the same level of performance as Pt-based catalysts [38]. There have only been a few reports on Ru-based electrocatalysts showing Pt-like activity. Mu and co-workers synthesized a novel N,P dual-doped carbon-encapsulated ruthenium diphosphide (RuP_2@NPC) nanoparticle electrocatalyst with an overpotential of 38 mV at 10 mA cm^{-2} [39]. Shao and co-workers prepared ruthenium nanoparticles modified on silicon nanowires (Ru/SiNWs) via directly reducing Ru ions with Si–H bonds, the Tafel slope and overpotential at 10 mA cm^{-2} of Ru/SiNWs is 81 mV/dec and 200 mV, respectively [40]. K. Philippot and co-workers synthesized a porous Ru nanomaterial with an overpotential of 83 mV at 10 mA cm^{-2} and a Tafel slope of 46 mV/dec [41]. In addition, the preparation method of Ru-based catalysts seem a little bit complication. (Delete this paragraph) In this study, we present a facile solvothermal approach to synthesize coral-like Ru/carbon (Ru/C) electrocatalyst with the assistance of 8-hydroxyquinoline (8-HQ). This catalyst exhibited excellent performance for HER. The overpotential of the Ru/C catalyst was found to be 41 mV at a current density of 10 mA/cm^2 and the Tafel slope was 46 mV/dec. Moreover, the Ru/C catalyst showed excellent stability in a 1000-cycle cyclic voltammetry (CV) test and in a 10-h chronoamperometry test.

2. EXPERIMENTAL

2.1. Reagents

All reagents were analytical grade, purchased from Sinopharm Chemical Reagent Co., Ltd., and used as received without purification.

2.2. Preparation of the coral-like Ru/C nanocomposites

The Ru/C catalyst was prepared via a one-pot solvothermal method with the assistance of 8-HQ. In a typical synthesis process, 1 g of F127 (carbon source and surfactant) was dissolved in a mixed solution of ethanol and ethanediol (v/v = 3:2, 15 mL). The mixture was stirred for 10 min at 40 °C until F127 was fully dissolved and a colourless transparent solution was obtained. Then, an appropriate amount of 8-HQ (chelating agent) was added to the aforementioned mixed solution. A transparent yellow solution was obtained when 8-HQ was completely dissolved. Next, 3 mL of $RuCl_3 \cdot 3H_2O$ ethanol solution (0.0037 g/mL of Ru) was added to the solution. After stirring for 4 h, the as-prepared solution was transferred into a 100 mL hydrothermal autoclave that was subsequently heated in an oven at 160 °C for 24 h.

After that, the autoclave was removed from the oven and naturally cooled to room temperature. The mixed solution was transferred to an open glass dish for evaporation at room temperature and then placed in an oven at 100 °C for 16 h. Finally, the dried material was scraped from the dish and calcined at 800 °C in a tube furnace at a heating rate of 2 °C/min. The obtained samples were denoted as Ru/C-x, where x represents the molar ratio of $8\text{-HQ}/Ru^{3+}$ in the sample. Depending on the amount of 8-HQ and the molar ratio of $8\text{-HQ}/Ru^{3+}$, the samples used in this study were denoted as Ru/C-0, Ru/C-5, Ru/C-10, and Ru/C-15.

2.3. Characterization

Powder X-ray diffraction (XRD) was performed on a D8 Advance apparatus using Cu Kα radiation (λ = 0.15418 nm), the measurement was carried out at an operating voltage of 40 kV and an operating current of 40 mA in the angular range 10–90° with a scan rate of 8°/min. N_2 adsorption–desorption isotherms were recorded using a Micromeritics ASAP 2020 sorptometer at liquid-nitrogen temperature (-196°C). Scanning electron microscopy (SEM) was performed on a NOVA NANOSEM 450 electron microscope. Transmission electron microscopy (TEM) was performed on a JEOL JEM-2010F field-emission microscope, the size distribution of the Ru particles was obtained by counting 100-150 particles in the TEM images. X-ray photoelectron spectroscopy (XPS) was measured using an ESCALAB 250Xi spectrometer equipped with Al Kα radiation (hv= 1486.6 eV) at a pressure of approximately 1×10^{-9} Torr. The actual content of Ru in the sample was determined by inductively coupled plasma atomic emission spectrometry (ICP-AES) on a Perkin-Elmer emission spectrometer.

2.4. Electrochemical Measurements

All electrochemical measurements were performed on a CHI 660D electrochemical station using a three-electrode system with 0.5 M H_2SO_4 aqueous solution as the electrolyte. A graphite rod was used as the counter electrode, and a saturated calomel electrode (SCE) was used as the reference electrode. Before the electrochemical measurements, the glassy carbon electrode that served as a catalyst supporter was first mechanically polished with a 0.05 μm alumina slurry and then washed with ethanol and deionized water to obtain a clean surface. The H_2SO_4 solution was saturated with N_2 for 30 min. The

working electrode was prepared as follows: 9 mg of catalyst sample was dispersed in a mixed solution of ethanol (600 µL) and Nafion (20 µL) to form a homogeneous suspension by sonication for 30 min. Then, 10 µL of the suspension was loaded onto the glassy carbon electrode and dried in air to obtain the working electrode (loading 0.75 mg cm^{-2}).

The HER activity of the catalyst was studied by LSV with a scan rate of 5 mV s^{-1}. Cyclic voltammograms (CV) were measured by measuring double layer capacitance (C_{dl}) in the potential of 0.1V to 0.3V (vs. RHE) with different scan rates (20-200 mV s^{-1}) to estimate the electrochemically active surface areas (ECSA). The electrochemical impedance spectroscopy (EIS) was tested from 0.1 to 10^5 Hz with an amplitude of 5 mV to study the electrode kinetics. The 1000-cycle CV stability test and chronoamperometry measurement were used to assess the stability of the catalysts. All the electrochemical tests were iR-corrected and performed at room temperature.

3. RESULTS AND DISCUSSION

3.1. Morphology and structure of Catalysts

The crystalline structure of the prepared Ru/C-x (x = 0, 5, 10, 15) samples were study by XRD. As shown in Fig. 1a, for each sample prepared with the assistance of 8-HQ (x = 5, 10, 15), the XRD pattern contains only one discernible diffraction peak at 44.0°, which was attributed to the (101) plane of the hexagonal close-packed phase of metallic Ru (0) [39]. The broad Ru peak suggests that the size of the Ru particles was relatively small and at the nanoscale [40,41], consistent with the particle size distribution obtained from the TEM analysis. However, when x = 0 (i.e., without 8-HQ), numerous peaks were observed at 38.4°, 42.1°, 44.0°, 58.3°, 69.4°, 78.4°, 84.7°, and 85.9°, which were ascribed to the (100), (002), (101), (102), (110), (103), (112), and (201) planes of Ru(0), respectively. Moreover, the (101) reflection peak at 44.0° was very strong, which attributed to severe aggregation of Ru nanoparticles on the carbon substrate in the absence of 8-HQ. This phenomenon is consistent with the SEM and TEM observations (Fig. 3a and Fig. 4a, respectively).

XPS was also used to reveal the chemical state of Ru. The Ru 3d core-level spectra have two spin-orbit components: Ru 3d$_{5/2}$ and Ru 3d$_{3/2}$. Notably, the binding energies of Ru 3d$_{3/2}$ and C1s are similar, which causes the Ru 3d$_{3/2}$ band to overlap with the C1s band. Therefore, Ru 3d$_{5/2}$ is generally chosen to determine the chemical state of Ru. Fig. 1b presents high-resolution XPS spectra of Ru 3d$_{5/2}$. The binding energy of Ru 3d$_{5/2}$ was approximately 280.2 eV, this value indicates that Ru in Ru/C-x (x = 0, 5, 10, 15) was in the zero-valent state [42-45]. The strongest Ru 3d$_{5/2}$ peak was observed when x = 10, which indicates that the maximum formation of Ru (0) was achieved when using an 8-HQ/Ru^{3+} molar ratio of 10. Because Ru (0) provides the catalytic active sites, Ru/C-10 should have the largest number of active sites, which is critical for the performance of the catalyst. The actual contents of Ru in the Ru/C-x catalysts were determined by ICP-AES, the results as summarized in Table 1, show that Ru/C-10 had the highest Ru content, which is consistent with the XPS results.
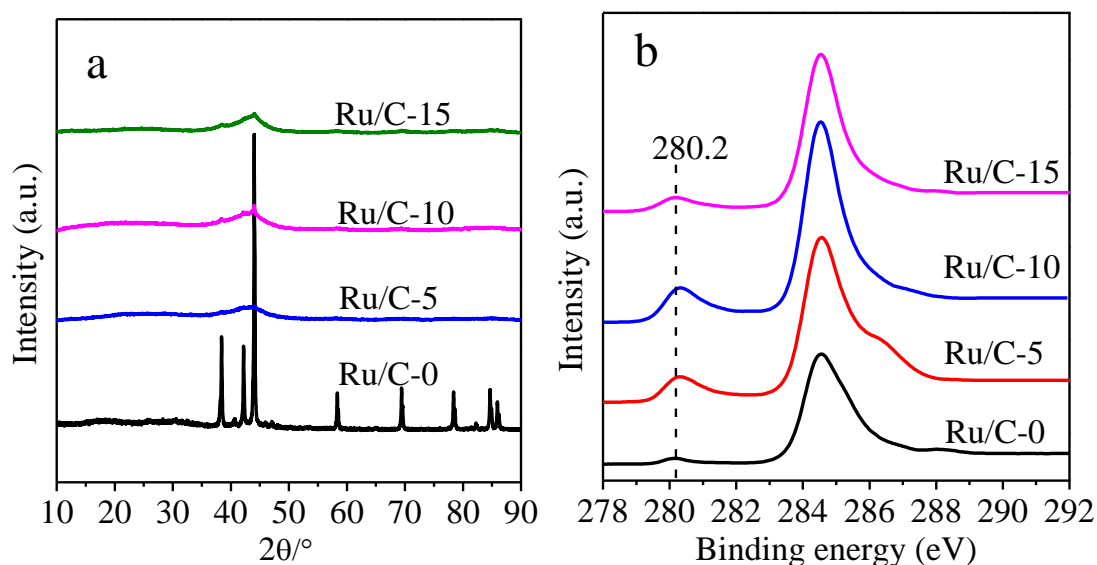
Figure 1. (a) XRD patterns of the prepared Ru/C–x samples. (b) High resolution XPS spectra of Ru $3d_{5/2}$.
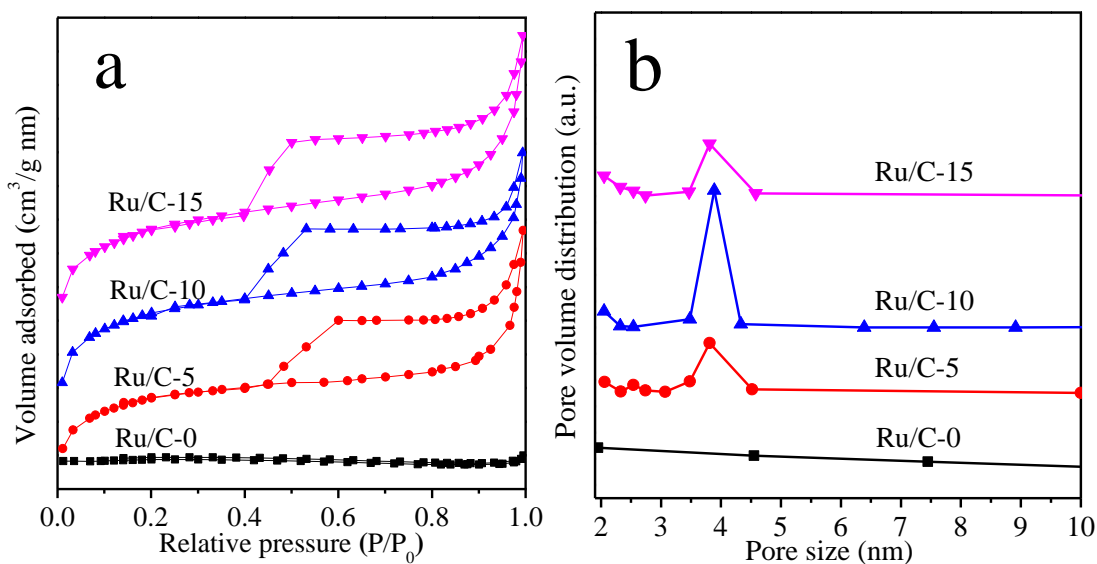

Figure 2. (a) Nitrogen adsorption−desorption isotherms and (b) BJH pore size distributions of the Ru/C-x catalysts.

The structure of the material has important influence on the performance of the material. N_2 sorption measurement was used to study the textural properties of the materials. Fig. 2 presents the N_2 adsorption–desorption isotherms and the BJH pore size distributions of the Ru/C-x (x = 0, 5, 10, 15) catalysts. When x = 5, 10, and 15 (with 8-HQ), all of the samples exhibited typical type IV curves with pronounced hysteresis, which was associated with the filling of microspores by capillary condensation. The results suggest that these samples exhibited large textural porosities and contained multiple-sized mesoporous [46,47]. The BJH pore size analysis (Fig. 2b) indicates that these materials possessed narrow

pore size distributions in the range of 3.5-4.5 nm, which is a typical distribution range for mesoporous structures. The large porosities led to a large specific surface area (Table 1). The large specific surface area, the textural pores, and the mesopores can facilitate mass transfer process in the HER. However, when x = 0, the sample showed a very small specific surface area and almost no pore structure, which was caused by the aggregation of the Ru nanoparticles. Therefore, 8-HQ is a very important factor in this study. Among all of the samples, Ru/C-10 exhibited the largest specific surface area and pore volume, which is beneficial to expose more active sites in the HER.

Table 1. Actual contents of Ru and textural properties of the prepared catalysts.

Samples	Ru (wt%)	S_{BET} (m^2/g)	V_p (cm^3/g)	D_p (nm)	D_a (nm)
Ru/C-0	5.3	2	/	/	/
Ru/C-5	21.0	198	0.12	3.8	2.4
Ru/C-10	22.3	264	0.16	3.8	2.5
Ru/C-15	11.6	98	0.06	3.6	2.6

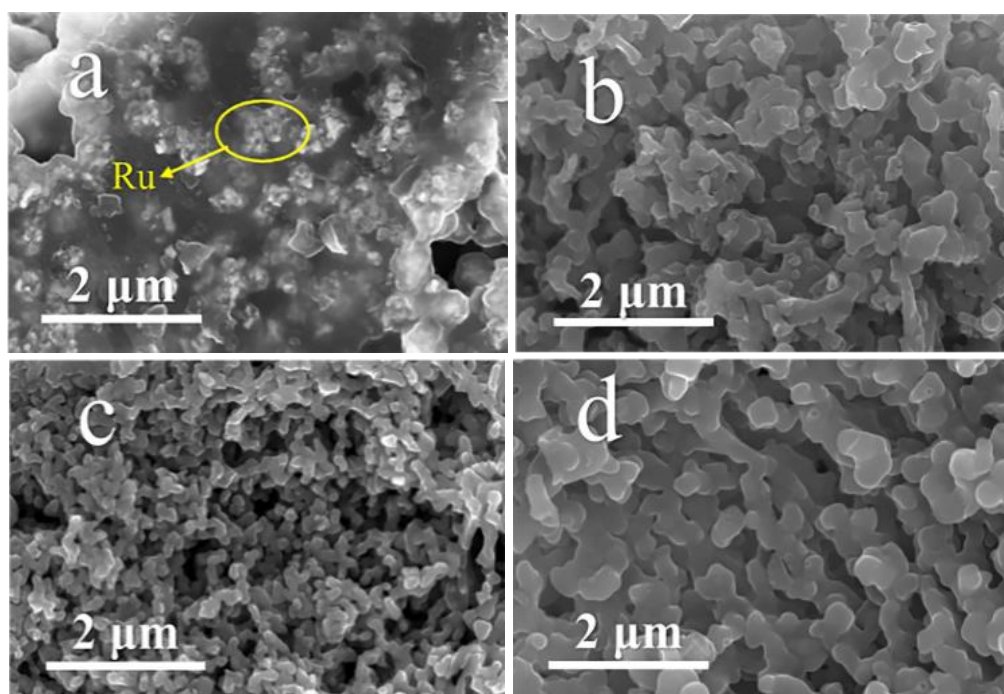**Figure 3.** SEM images of the Ru/C- x: (a) x = 0, (b) x = 5, (c) x = 10, (d) x = 15.

The morphology of the prepared samples was characterized by SEM. As shown in Fig. 3a, Ru particles were obviously aggregated when the chelating agent 8-HQ was not used, this result indicates that 8-HQ can effectively prevent the aggregation of Ru particles. When x = 5 (Fig. 3b), the sample exhibited an irregular morphology, such morphology is not beneficial to electron transfer during the reaction. When x = 10, the morphology of the sample became more regular and exhibited a coral-like structure, the particle size also decreased greatly. When x = 15, the sample maintained the regular coral-like structure, but the particle size increased substantially, this increase in particle size resulted in a

relatively small specific surface area of Ru/C-15, which further led to a decreased number of active sites and reduced catalytic activity. Ru/C-10 exhibited the best coral-like structure and the smallest particle size. The unique structure and small particle size not only enhanced the electron-transfer capability but also increased the specific surface area of this sample.
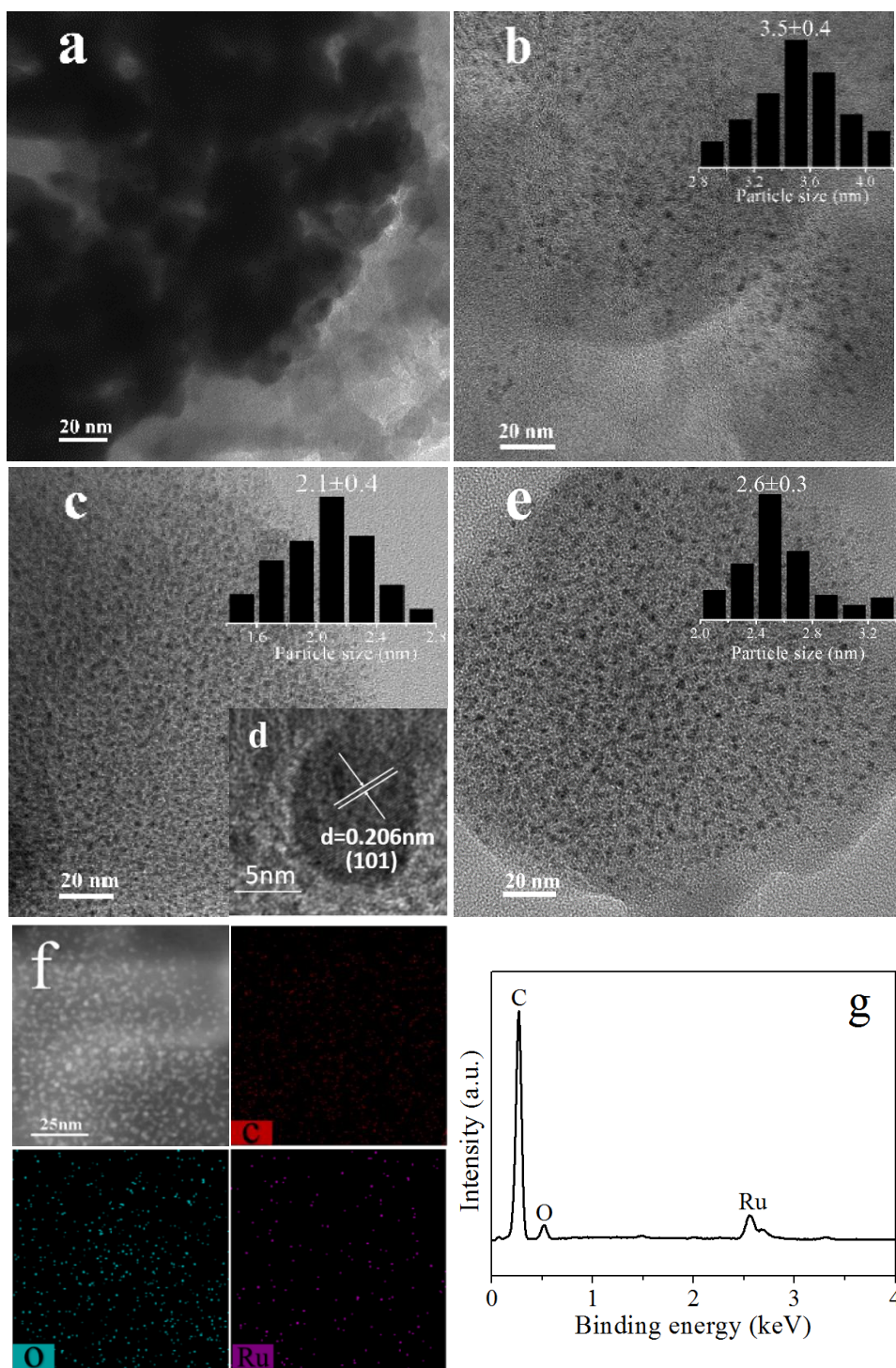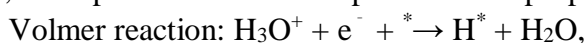

Figure 4. (a) TEM of the Ru/C-0. (b) TEM of the Ru/C-5. (c) TEM of the Ru/C-10. (d) High-resolution TEM image of Ru/C-10. (e) TEM of the Ru/C-15. (f) STEM mapping of Ru/C-10. (g) STEM–EDX of Ru/C-10.

The precise morphology and crystal microstructure of the samples were further characterized by TEM and high-resolution TEM (HRTEM). The image in Fig. 4a shows that Ru/C-0 exhibited severe aggregation of Ru particles, consistent with the previous results. When x = 5, 10, and 15 (Fig. 4b-4e), the Ru nanoparticles were uniformly distributed on the carbon substrate. However, the size distribution of Ru particles depended on the molar ratio of 8-HQ/Ru^{3+}. When x = 10, the size of the Ru particles was the smallest, approximately 2.1 nm, and the distribution was relatively uniform. In general, the size of the nanoparticles is critical for the performance of the catalyst, reducing the size of the nanoparticles can dramatically increase the number of surface active sites [48]. The HRTEM image of Ru/C-10 (Fig. 4d) shows that the lattice fringe spacing was 0.206 nm, which corresponds to the Ru (101) crystal plane [39]. This result is in agreement with the XRD results. The distribution of elements was further analysed by STEM. The elemental mapping images for the representative Ru/C-10 sample (Fig. 4f) reveal that C, O, and Ru were distributed homogeneously throughout the sample.

3.2. Electrocatalytic performance

The electrocatalytic performance of the samples was first studied by linear sweep voltammetry (LSV). The measurements were carried out using a typical three-electrode system with a 0.5 M H_2SO_4 aqueous solution as the electrolyte, the scan rate was 5 mV/s. For comparison purposes, commercial 20 wt% Pt/C catalyst was also tested under the same conditions. As shown in Fig. 5a, the performance of Ru/C-10 was most similar to that of the commercial Pt/C catalyst. To drive 10 mA/cm^2, Ru/C-10 required an overpotential of only 41 mV, this value was smaller than that of the other samples. This result indicates that Ru/C-10 exhibited excellent electrocatalytic performance for the HER. Given the previous characterization results, we speculate that Ru/C-10 has the largest specific surface area, the best coral-like morphology, and the smallest Ru nanoparticles. These properties not only provide the largest number of catalytic active sites but also facilitate electron transfer, resulting in Ru/C-10 exhibiting the best catalytic performance among the prepared catalysts.

To reveal the reaction mechanism of the HER catalysed by Ru/C, the Tafel slope was calculated via the Tafel equation ($\eta = a + b \log j$) [49], where η represents the overpotential, b represents the Tafel slope, and j represents the current density. HER is a multi-step electrochemical process on the electrode surface, three possible reaction steps have been proposed for the HER in an acid electrolyte:

Volmer reaction: $H_3O^+ + e^- + ^* \rightarrow H^* + H_2O$,

$b \approx 120$ mV   (1)

Heyrovsky reaction: $H_3O^+ + e^- + H^* \rightarrow H_2 + H_2O$

$b \approx 40$ mV (2)

Tafel reaction: $H^* + H^* \rightarrow H_2$

$b \approx 30$ mV   (3)

The HER is generally agreed to start with the Volmer reaction (Equation (1)), a hydrated proton combines an electron and attaches on the catalyst (*). Then, the adsorbed H (H^*) will through Heyrovsky reaction or Tafel reaction to form H_2. As for the Heyrovsky reaction, a hydrated proton combines H^* and receive an electro to form H_2 on the catalyst surface (Equation (2)). In addition, two H^* can combine to

form hydrogen directly, which is known as Tafel reaction (Equation (3)). Thus, the possible HER mechanisms based on these three steps are the Volmer–Heyrovsky and the Volmer–Tafel reaction sequences. As shown in Fig. 5b, a Tafel slope of 46 mV/dec was determined for Ru/C-10 from the low-scan-rate polarization curve and the Tafel equation, which is similar to the Tafel slope of commercial Pt/C (34 mV/dec). This value suggests that the HER followed the Volmer-Heyrovsky mechanism and the Heyrovsky step is the rate determining step. Ru/C-10 had the lowest Tafel slope among all the samples, which suggests that Ru/C-10 exhibited the best kinetic performance. The HER activity of Ru/C-10 and other electrocatalysts are shown in Table 2.

Table 2. Comparison of HER activity of Ru/C-10 with other HER electrocatalysts.

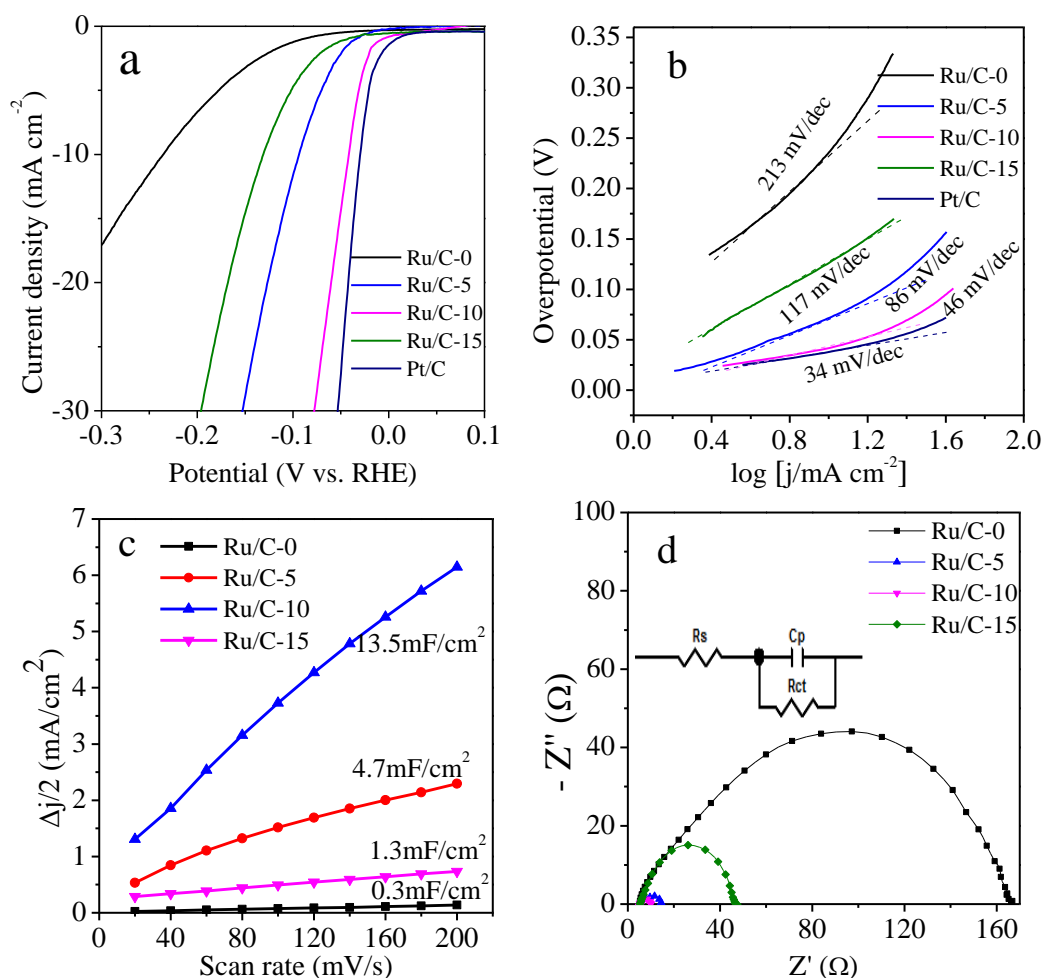| Catalyst	Overpotential@j (mV@mA cm^{-2})	Tafel Slope (mV dec^{-1})
Ru/SiNW	200 @10	81 [50]
Ru/MeOH/THF	83 @10	46 [51]
NiCoP@Ru	49 @10	49 [52]
Ru/C-10	41 @10	46 [This work]
Pt/C	33 @10	34 [This work]

Figure 5. (a) LSV curves of Ru/C-x. (b) Corresponding Tafel slopes of catalysts. (c) Estimated Cdl of Ru/C-x. (d) Nyquist curves for the Ru/C-x.

The overpotential and Tafel slope of Ru/C-10 in this work are lower than the reported values for other Ru-based electrocatalysts as shown in Table 2, suggesting Ru/C-10 has better HER activity.

Furthermore, we further investigated the electrochemically active surface area (ECSA), which can be calculated by the formula ECSA = C_{dl} /Cs [53]. Cdl is a standard scale used to estimate the interfacial area between the electrolyte and the electrode surface [54], and the the Cs represents the capacitive behavior of the as-prepared electrode. It can be seen that the Cdl is expected to be linearly proportional to the ECSA, the larger the Cdl is, the larger the ECSA. During the HER, the CV curves were acquired in the range from 0.1 to 0.3 V (vs. RHE) at different scan rates to calculate the Cdl. As shown in Fig. 5c, the Cdl of Ru/C-10 was 13.5 mF/cm^2, which was the highest among the investigated samples, the higher C_{dl} value indicates the high exposure of active edge sites in Ru/C-10 sample. Electrochemical impedance spectroscopy (EIS) is an important approach to study the HER reaction kinetics (Fig. 5d). To obtain the EIS parameters, we constructed the corresponding equivalent circuit shown in the inset of Fig. 5d. The charge transfer resistance Rct is represented by the diameter of the semicircle in the Nyquist plot. The smaller the value of Rct is, the easier the electron flow and the easier the HER reaction proceeds [55]. As shown in Fig.5d, the Nyquist plots show that Ru/C-10 has smaller charge transfer resistance obtained from the semicircle in the high-frequency zone. These results indicate that the charge transfer kinetics is greatly accelerated when the molar ratio of 8-HQ/Ru^{3+} is 10.

The long-term stability and durability of catalyst are important factors for their practical application. In this study, a 1000-cycle CV stability test and chronoamperometry measurement were used to assess the stability and durability of the samples. The CV test was performed in the range from -0.16 to 0.24 V (vs. RHE) at a scan rate of 100 mV/s on the Ru/C-10 sample. Fig. 6a shows that the polarization curves were almost coincident before and after 1000 CV cycles, which demonstrates excellent stability of the samples. The chronoamperometry results are shown in Fig. 6b, the chronoamperometry measurement reveals that Ru/C-10 has a slight loss of cathodic current density after running for 10 h at a constant overpotential of 55 mV vs. RHE. This demonstrates that the Ru/C-10 catalyst exhibited superior durability.
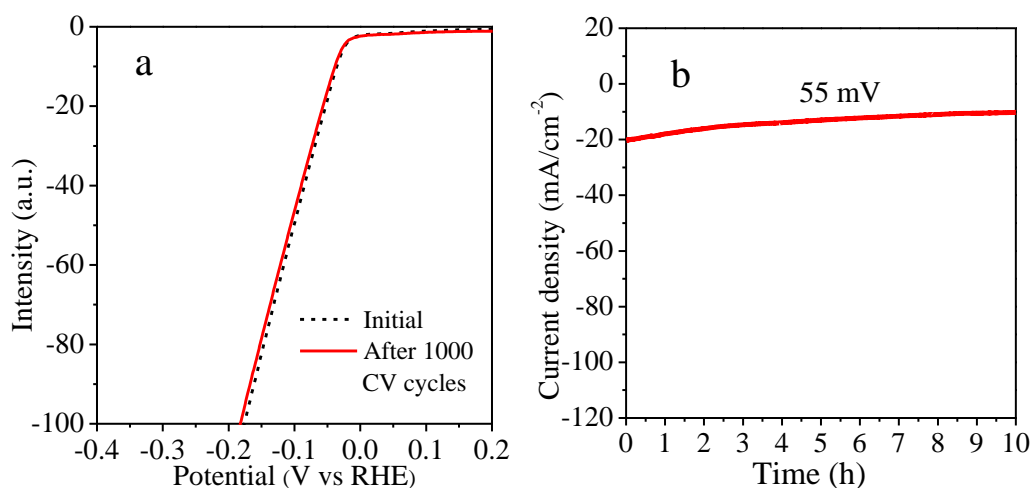

Figure 6. (a) Polarization curves recorded for Ru/C-10 before and after 1000 CV cycles in 0.5M H$_2$SO$_4$ solution. (b) Time-dependent current density curve of the Ru/C-10 under static overpotential of 55 mV vs. RHE for 10 h.

4. CONCLUSION

In this study, a highly effective coral-like Ru/C electrocatalyst was synthesized via a facile solvothermal approach with the assistance of 8-HQ. This catalyst exhibited excellent electrocatalytic performance for the HER, the superior performance of catalyst was attributed to the large specific surface area, ultrafine ruthenium nanoparticles and the unique regular coral-like structure. These properties not only promote the reaction by facilitating the electron transfer but also exposure more catalytic active sites, which increases the activity of the catalyst. In our work, this novel method opens a new avenue to synthesize ruthenium-based catalysts and shows that Ru/C catalyst is a promising alternative to commercial Pt/C as HER catalyst in future energy applications.

References

1. J. J. Li, X. X. Han, M. Wang, Y. Zhao and C. Dong, *New J. Chem.*, 42 (2018) 4114.
2. V. Barough, E. S. Iranizad, A. Bayat, and K. Hemmati, *J. Electroanal. Chem.*, 823 (2018) 278.
3. K. Lan, X. Wang, H. D. Yang, K. lqbal, Y. Zhu, P. B. Jaing, Y. Tang, Y. Y. Yang, W. B. Gao, and R. Li, *ChemElectroChem*, 5 (2018) 1.
4. Q. Z. Wang, J. J. He, Y. B. Shi, S. l. Zhang, T. J. Niu, H. D. She, Y. P. Bi and Z. Q. Lei, *Appl. Catal., B*, 214 (2017) 158.
5. S. Saha, K. Ojha, M. Sharma and A. K. Ganguli, *New J. Chem.*, 41 (2017) 5916.
6. X. X. Zou and Y. Zhang, *Chem. Soc. Rev.*, 44 (2015) 5148.
7. Y. F. Yang, H. Yang, C. J. Liang and X. Zhu, *Int. J. Electrochem. Sci.*, 13 (2018) 7193.
8. J. Wang, W. Cui, Q. Liu, Z. Xing, A. M. Asiri and X. Sun, *Adv. Mater.*, 28 (2016) 215.
9. S. T. Hunt, M. Milina, Z. S. Wang and Y. Roman-Leshkov, *Energy Environ. Sci.*, 9 (2016) 3290.
10. M. Gong, D. Y. Wang, C. C. Chen, B. J. Hwang and H. Dai, *Nano Res.*, 9 (2016) 28.
11. Y. Zheng, Y. Jiao, Y. H. Zhu, L. H. Li, Y. Han, Y. Chen, A. J. Du, M. Jaroniec and S. Z. Qiao, *Nat. Commun.*, 5 (2014) 3783.
12. M. Chhetri, S. Maitra, H. Chakraborty, U. V. Waghmare and C. N. R. Rao, *Energy Environ. Sci.*, 9 (2016) 95.
13. Y. Ito, W. T. Cong, T. Fujita, Z. Tang and M. W. Chen, *Angew. Chem., Int. Ed.*, 54 (2015) 2131.
14. M. Zhang, R. Q. Li, D. Hu, X. F. Huang, Y. Q. Liu and K. Yan, *J. Electroanal. Chem.*, 836 (2019) 102.
15. J. Q. Tian, Q. Liu, A. M. Asiri and X. Sun, *J. Am. Chem. Soc.*, 136 (2014) 7587.
16. E. J. Popczun, C. G. Read, C. W. Roske, N. S. Lewis and R. E. Schaak, *Angew. Chem. Int. Ed.*, 53 (2014) 5427.
17. Z. H. Pu, I. S. Amiinu, Z. K. Kou, W. Q. Li and S.C. Mu, *Angew. Chem.*, 129 (2017) 11717.
18. Q. Liu, J. Q. Tian, W. Cui, P. Jiang, N. Y. Cheng, A. M. Asiri and X. P. Sun, *Angew. Chem., Int. Ed.*, 53 (2014) 6710.

19. D. M. Fernandes, M. P. Araujo, A. Haider, A. S. Mougharbel, A-J. S. Fernandes, U. Kortz and C. Freire, *ChemElectroChem*, 4 (2017) 1.
20. W. Zhou, J. Jia, J. Lu, L. Yang, D. Hou, G. Li and S. Chen, *Nano Energy*, 28 (2016) 29.
21. N. Du, C. Wang, X. Wang, Y. Lin, J. Jiang and Y. Xiong, *Adv. Mater.*, 28 (2016) 2077.
22. J. Chang, Y. Xiao, M. Xiao, J. Ge, C. Liu and W. Xing, *ACS Catal.*, 5 (2015) 6874.
23. X. Long, G. X. Li, Z. L. Wang, H. Y. Zhu, T. Zhang, S. Xiao, W. Guo and S. H. Yang, *J. Am. Chem. Soc.*, 137 (2015) 11900.
24. D. W. Mulder, Y. Guo, M. W. Ratzloff and P. W. King, *J. Am. Chem. Soc.*, 139 (2017) 83.
25. M. Caban Acevedo, M. L. Stone, J. R. Schmidt, J. G. Thomas, Q. Ding, H. C. Chang, M. L. Tsai, J. H. He and S. Jin, *Nat. Mater.*, 14 (2015) 1245.
26. J. Y. Zhang, B. R. Xiao, X. L. Liu, P. Liu, P. Xi, W. Xiao, J. Ding, D. Gao and D. Q. Xue, *J. Mater. Chem. A.*, 5 (2017) 17601.
27. Y. M. Tian, J. Yu, H. S. Zhang, C. Wang, M. Zhang, Z. W. Lin and J. Wang, *Electrochim. Acta*, 300 (2019) 217.
28. A. Sivanantham, P. Ganesan and S. Shanmugam, *Adv. Funct. Mater.*, 26 (2016) 4661.
29. D. Xue, S-P. Luo and S-Z. Zhan, *New J. Chem.*, 41 (2017) 8503.
30. S. Xu, S. Chu, L. Yang, Y. Chen, Z.Wang and C. Jiang, *New J. Chem.*, 42 (2018) 19557.
31. P. Thangasamy, N. Ilayaraja, D. Jeyakumar and M. Sathish, *Chem. Commun.*, 53 (2017) 2245.
32. A. M. Gómez–Marín and E. A. Ticianelli, *Appl. Catal. B: Environ.*, 209 (2017) 600.
33. Y. S. Jin, H. Wang, J. J. Li, X. Yue, Y. J. Han, P.K. Shen and Y. Cui, *Adv. Mater.*, 28 (2016) 3785.
34. T. X. Wu, G. Z. Wang, Y. X. Zhang, S.H. Kang and H. M. Zhang, *New J. Chem.*, 41 (2017) 7012.
35. X. H. Gao, G. T. Yu, L. Zheng, C. M. Zhang, H. Li, T. Wang, P. D. An, M. Liu, X. Q. Qiu and W. Chen, *Appl. Energy Mater.*, 2 (2019) 966.
36. M. Yuan, Y. C. Zhu, L. Deng, R. X. Ming, A. L. Zhang, W. Y. Li, B. Chai and Z. D. Ren, *New J. Chem.*, 41 (2017) 6152.
37. Q. Song, X. Z. Qiao, L. Z. Liu, Z. J. Xue, C. H. Huang, and T. Wang, *Chem. Commun.*, 55 (2019) 965.
38. W. D. Li, Y. Liu, X. L. Feng, Y. Shang, X. Yong, T. L. Feng, Z. Y. Liu, B. J. Li, Z. M. Chen, S. Y. Lu, and B. Yang, *Adv. Mater*, 30 (2018) 1800676.
39. Z. Chen, J. F. Lu, Y. Ai, Y. F. Ji and L. J. Wan, *ACS Appl. Mater. Interfaces.*, 8 (2016) 35132.
40. H. Y. Liang, G. Z. Chen, S. Desinan, R. Rose, F. Rosei and D. L. Ma, *Int. J. Hydrogen Energy.*, 37 (2012) 17921.
41. G. Z. Chen, S. Desinan, R. Rosei and D. L. Ma, *Chem. Commun.*, 48 (2012) 8009.
42. C. X. Zhang, H. J. Tao, Y. M. Dai, X. C. He and K. J. Zhang, *Prog Nat SCI-Mater.*, 24 (2014) 671.
43. R. Q. Ye, Y. Y. Liu, Z. W. Peng, T. Wang, A. S. Jalilov, B. I. Yakobson, S-H Wei and J. M. Tour, *ACS Appl. Mater. Interfaces.*, 9 (2017) 3785.
44. Y. T. Li, F. Q. Chu, Y. Liu, Y. Kong, Y. X. Tao, Y. X. Li and Y. Qin, *Chem. Commun.*, 54 (2018) 13076.
45. Y. L. Ma, X. J. Li, Y. Zhang, L. Chen, J. T. Wu, D. G. Gao, J. Bi, and Y. Fan, *J. Alloys Compd.*, 708 (2017) 270.
46. Y. C. Wang, S. Y. Tao, Y. L. An, S. Wu and C. G. Meng, *J. Mater. Chem. A.*, 1 (2013) 8876.
47. Y. H. Deng, C. Liu, T. Yu, F. Liu, F. Q. Zhang, Y. Wan, L. J. Zhang, H. T. Wang and D. Y. Zhao, *Chem. Mater.*, 19 (2007) 3271.
48. C. L. Xu, M. Ming, Q. Wang, C. Yang, G. Y. Fan, Y. Wang, D. G. Gao, J. Bi and Y. Zhang, *J. Mater. Chem. A.*, 6 (2018) 14380.
49. J. Wang, F. Xu, H. Y. Jin, Y. Q. Chen, and Y. Wang, *Adv. Mater.*, 29 (2017) 1605838.
50. L. L. Zhu, Q. Cai, F. Liao, M. Q. Sheng, and M. W. Shao, *Electrochem. Commun.*, 52 (2015) 29.
51. S. Drouet, J. Creus, V. Collière, J. Garcıa-Anton, X. Sala, and K. Philippot, *Chem. Commun.*, 53 (2017) 11713.
52. S. L. Liu, Q. P. Liu, Y. Lv, B. Y. Chen, Q. Zhou, L. Wang, Q. H. Zheng, C. J. Che and C. Y. Chen,

Chem. Commun., 53 (2017) 13153.
53. Y. Yang, Z. Y. Lun, G. L. Xia, F. C. Zheng, M. N. He, and Q. W. Chen, *Energy Environ. Sci.*, 8 (2015) 3563.
54. X. L. Chen, J. Zheng, X. Zhong, Y. H. Jin, G. L. Zhuang, X. N. Li, S. W. Deng and J-G Wang, *Catal. Sci. Technol.*, 7 (2017) 4964.
55. B. Santosh, Z. Q. Wu. R. S. Siddhartha, G. K. Prasad, S. S. Ramamurthy and S. Mitra, *Int. J. Hydrogen Energy*, 41 (2016) 23007.